13th World Conference on Earthquake Engineering
Vancouver, B.C., Canada
August 1-6, 2004
Paper No. 555

MODELING OF SLENDER REINFORCED CONCRETE WALLS

Kutay ORAKCAL[1] **and John W. WALLACE**[2]

SUMMARY

This study investigates the effectiveness of a wall macro-model in predicting the flexural nonlinear response of reinforced concrete (RC) structural walls. Model results are compared with experimental results for slender RC walls with rectangular and T-shaped cross sections. The analytical model is calibrated and the test measurements are processed to allow for a direct comparison of the predicted and measured flexural responses. Responses are compared at various locations on the walls. Results obtained with the analytical model for rectangular wall cross sections compare favorably with experimentally responses for flexural capacity, stiffness, and deformability, although some significant variation is noted for local compression strains. For T-shaped walls, the agreement between model and experimental results is reasonably good, although the model is unable to capture the variation of the longitudinal strains along the flange. Overall, the wall model developed and the calibration studies conducted allow for improved prediction of the cyclic response of slender reinforced concrete shear walls.

INTRODUCTION

Prediction of the inelastic response of reinforced concrete (RC) structural walls and wall systems requires accurate, effective, and robust modeling and analysis tools that incorporate important material characteristics and behavioral response features such as neutral axis migration, tension-stiffening, progressive gap closure, confinement, nonlinear shear behavior, and the effect of fluctuating axial force on strength and stiffness. Effective analytical models should be relatively simple to implement and reasonably accurate in predicting the hysteretic responses of RC walls at both local and global levels, as well as capturing the interaction of the walls with other structural members.

Various phenomenological macroscopic models have been proposed in order to incorporate such response features in predicting the inelastic response of RC structural walls. The Multi-Component-in-Parallel Model (MCPM, later referred to as Multiple-Vertical-Line-Element Model, MVLEM) proposed by Vulcano [1] has been shown to successfully capture important response characteristics via the simplicity of a macroscopic model. Yet, the model has not been implemented into widely available computer

[1] Graduate Research Assistant, Department of Civil & Environmental Engineering, University of California Los Angeles, USA.
[2] Associate Professor, Department of Civil & Environmental Engineering, University of California Los Angeles, USA.

programs, and has not been sufficiently calibrated with and validated against extensive experimental data at both local and global response levels.

Given these shortcomings, a research project was undertaken to investigate and improve the MVLEM for RC wall systems, as well as to calibrate and validate it against experimental data. A description of the improved model, implementation of detailed cyclic constitutive relationships, and the sensitivity of the model predictions to both model and material parameters are presented by Orakcal [2]. This paper emphasizes the accuracy and limitations of the model by comparing model results with experimental results. The study presented herein focuses on modeling and simulation of the flexural response.

THE ANALYTICAL MODEL

A brief description of the wall model and implemented constitutive relationships are presented in this section. The model in Fig. 1(a) is an implementation of the generic MVLE model for structural walls. A structural wall is modeled as a stack of *m* elements, which are placed one upon the other (Fig. 1(b)). The flexural response is simulated by a series of uniaxial elements (or macro-fibers) connected to infinitely rigid beams at the top and bottom (e.g., floor) levels. A single MVLE model has six global degrees of freedom, three each located at the center of the rigid top and bottom beams. The primary simplification of the model involves applying the plane-sections-remain-plane assumption in calculating the strain level in each uniaxial element according to values of displacement or rotation at the degrees of freedom of each wall element. The stiffness properties and force-displacement relationships of the uniaxial elements are defined according to constitutive stress-strain relationships implemented in the model for concrete and steel and the tributary area assigned to each uniaxial element. The strains in concrete and steel are typically assumed equal (perfect bond) within each uniaxial element.

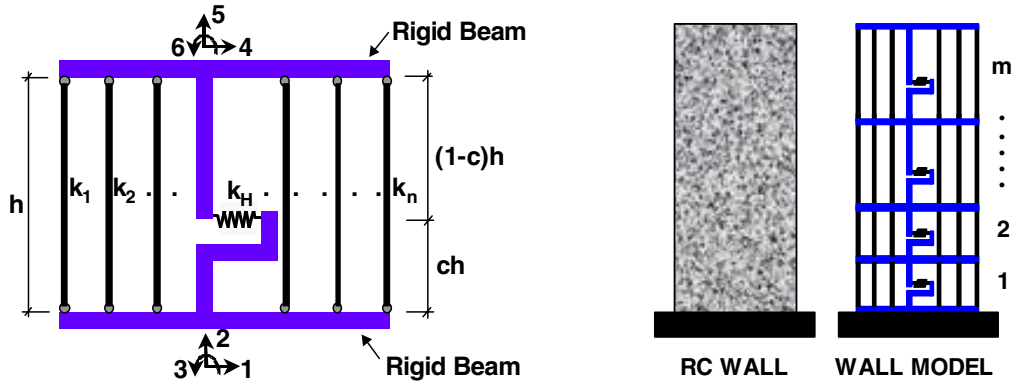

(a) MVLEM Element **(b) Model of a Wall**

Figure 1 Multiple-Vertical-Line-Element Model

The relative rotation between top and bottom faces of the wall element occurs around the point placed on the central axis of the element at height *ch*. A suitable value of the parameter *c* is based on the expected curvature distribution along the element height *h*, although an accurate assessment of *c* is not necessary if a moderate number of wall elements are used within the yielding region (Orakcal [2]). A horizontal spring placed at the height *ch*, with a nonlinear hysteretic force-deformation behavior following an origin-oriented hysteresis model (OOHM) (Kabeyasawa [3]) was originally suggested by Vulcano [1] to simulate the shear response of the wall element. The OOHM was proven to be unsuitable by Vulcano [4] for an accurate idealization of the shear hysteretic behavior especially when high shear stresses are expected. However, this study focuses on modeling of the flexural response, thus a linear elastic force-deformation

behavior was adopted for the horizontal "shear" spring. For the present model, flexural and shear modes of deformation of the wall member are uncoupled (i.e., flexural deformations do not affect shear strength or deformation), and the horizontal shear displacement at the top of the element does not depend on *c*.

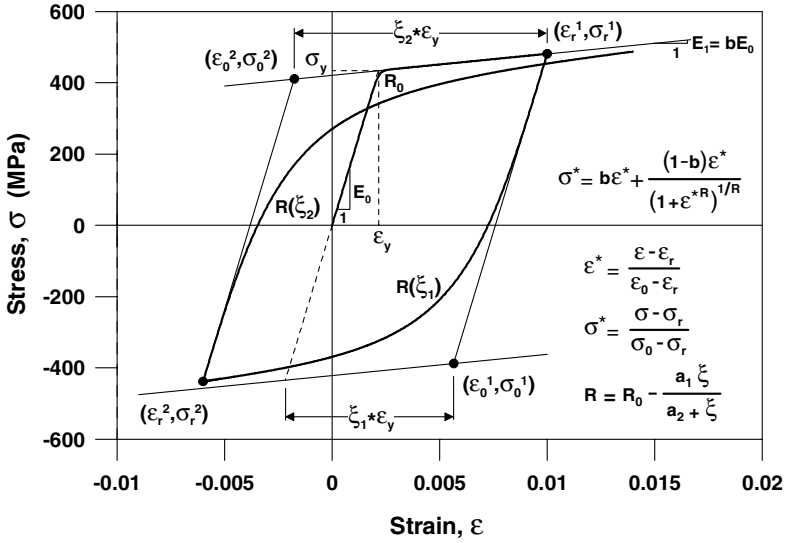

Figure 2 Constitutive Model for Reinforcing Steel

The reinforcing steel stress-strain behavior implemented in the wall model is the well-known nonlinear relationship of Menegotto [5] (Fig. 2), as extended by Filippou [6] to include isotropic strain hardening effects. The hysteretic constitutive relation developed by Chang [7] (Fig. 3) is used as the basis for the relation implemented for concrete, because it is a generalized constitutive model that allows recalibration or updating of model parameters based on available experimental data. The model provides the flexibility to represent the hysteretic behavior of confined and unconfined concrete in both cyclic compression and tension, with particular emphasis paid to the transition between crack opening and closure. The constitutive relationships implemented in this study can be controlled and calibrated to follow the relations developed by Belarbi [8] or similar empirical relations to model tension stiffening. Details of the constitutive models and the sensitivity of the analytical results to model parameters are presented by Orakcal [2].

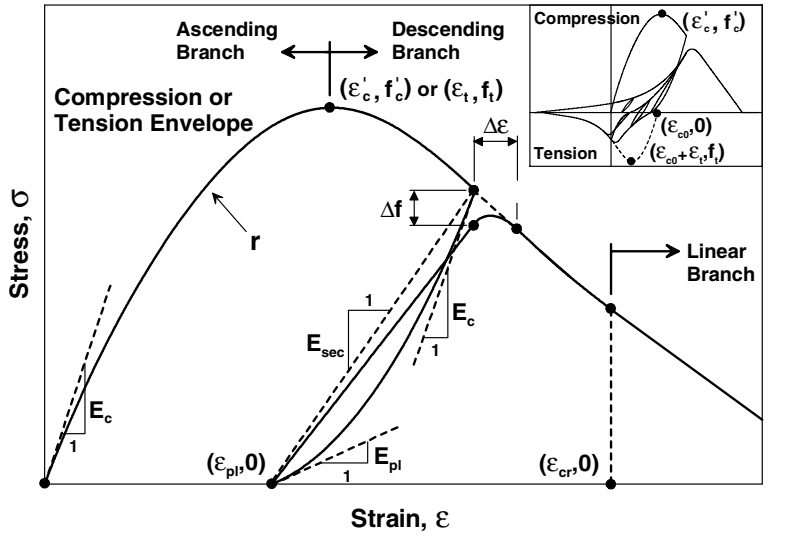

Figure 3 Constitutive Model for Concrete

EXPERIMENTAL RESULTS

Experimental results were obtained for four, approximately quarter-scale wall specimens tested by Thomsen [9,10]. The walls tested included two walls with rectangular cross sections (RW1, RW2), and two walls with T-shaped cross sections (TW1, TW2), with the primary variable in the test program being the level of detailing provided at the wall boundaries. A brief overview of these studies is provided in the following paragraphs, with more detailed information concerning the walls presented in Thomsen [9,10] and Massone [11].

Test Specimen Information

The walls were 3.66 m tall and 102 mm thick, with web and flange lengths of 1.22 m. Floor slabs were provided at 0.914 m intervals over the height of the T-shaped walls. Typical material properties were selected for design, i.e., f_c' = 27.4 MPa and σ_y = 414 MPa. Boundary vertical steel consisted of 8 - #3 (d_b = 9.53 mm) bars, whereas web bars were deformed #2 (d_b = 6.35 mm). Detailing requirements at the boundaries of the wall specimens were evaluated using the displacement-based design approach presented by Wallace [12,13]. Well-detailed boundary elements were provided at the edges of the walls over the bottom 1.22 m of each wall. A capacity design approach was used to avoid shear failure and favorable anchorage conditions existed for the vertical reinforcement anchored within the pedestal at the base of the wall. Sample reinforcing details for a rectangular wall specimen RW2 and for a T-shaped wall specimen TW2 are shown in Fig. 4.

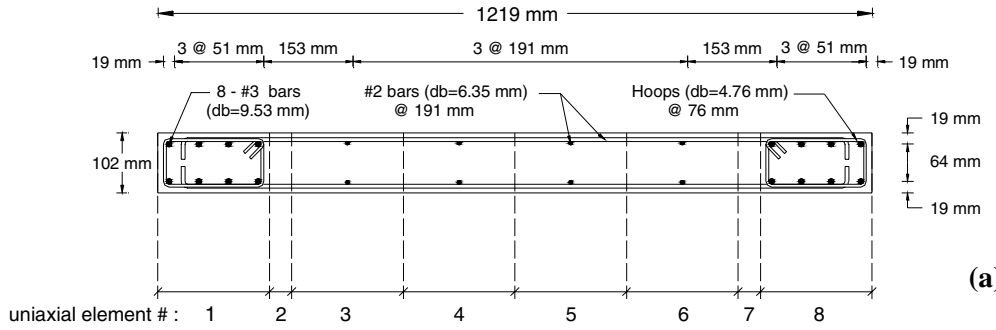

(a) Wall RW2

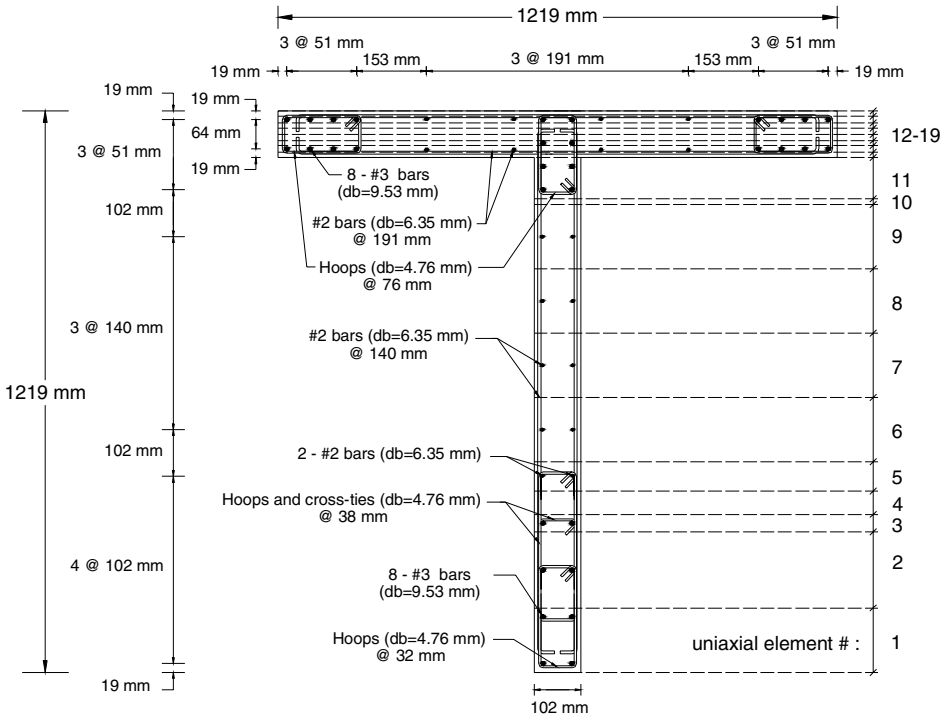

(b) Wall TW2

Figure 4 Wall Cross Sectional Views and Model Discretization

Testing and Instrumentation

The wall specimens were tested in an upright position. An axial load of approximately $0.10\,A_g f_c'$ was applied at the top of the wall by hydraulic jacks mounted on top of the load transfer assembly. The axial stress was applied prior to imposing lateral displacements, and held constant throughout the duration of each test. Cyclic lateral displacements were applied to the walls using a hydraulic actuator mounted horizontally to a reaction wall 3.81 m above the base of the wall. Out-of-plane support was provided to prevent twisting of the wall specimen during testing.

Instrumentation was used to measure displacements, loads, and strains at critical locations for each wall specimen (Fig. 5). Four wire potentiometers (WPs) were mounted to a rigid steel reference frame to measure lateral displacements at 0.91 m intervals over the wall height. A linear potentiometer was also mounted horizontally on the pedestal to measure any horizontal slip of the pedestal along the strong floor. Two additional linear potentiometers were mounted vertically at each end of the pedestal to measure rotation caused by uplift of the pedestal from the strong floor. Shear deformations were measured through the use of wire potentiometers mounted on the bottom two stories (in an "X" configuration) of each specimen (Fig. 5).

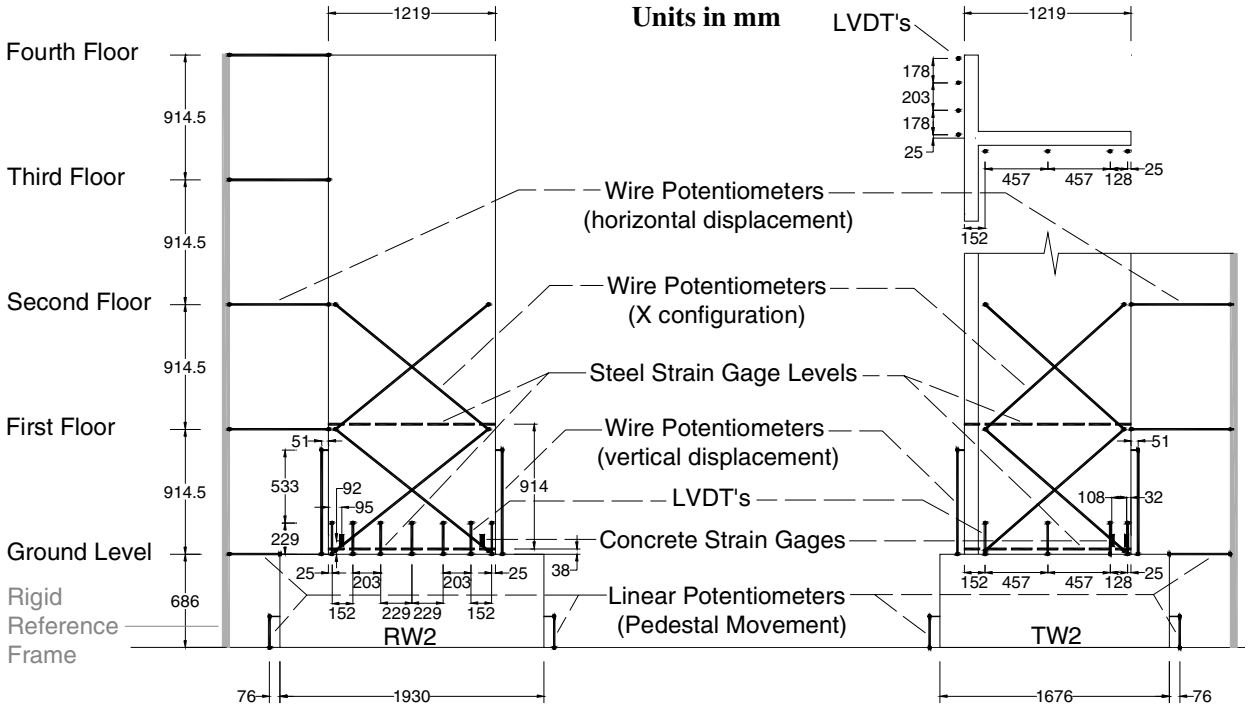

Figure 5 Instrumentation on the Wall Specimens

Wall base rotations were obtained by taking the difference in the axial (vertical) displacements measured by the two wire potentiometers mounted between the base and first story level at each end of the wall and dividing the difference in relative axial displacements by the distance between the potentiometers. Linear variable differential transducers (LVDTs) were mounted vertically (Fig. 5), over a gage length of 229 mm, at various locations along the web and flange of each wall so that axial strains and section curvatures could be calculated. The rectangular walls were instrumented with seven LVDTs spaced along the length of the wall; whereas, the T-shaped walls had four LVDTs mounted along the web and five mounted along the outside face of the flange. Axial concrete strains within the boundary regions of specimens RW2 and TW2 also were measured using embedded concrete strain gauges. The center of these gauges were located

approximately 92 mm above the pedestal interface, with one gauge in each boundary element for RW2, whereas TW2 had two gauges in the web boundary element. The strains in the reinforcing steel also were measured through the use of strain gauges at wall base and first story levels (1.22 m above the pedestal-wall interface). All three types of reinforcement were monitored (longitudinal, uniformly distributed web, and transverse boundary) at various locations (see Thomsen [9]).

CALIBRATION OF THE ANALYTICAL MODEL

In this paper, calibration of the analytical model and comparison of analytical and experimental results is limited to the rectangular wall specimen RW2 and the T-shaped wall specimen TW2; because specimens RW2 and TW2 were observed to withstand many cycles of inelastic deformation until failure. In the following paragraphs, calibration of model and material parameters are described.

Calibration for Geometry

Figure 4 displays possible model configurations, with 8 elements stacked upon each other (m = 8); with 8 uniaxial elements defined along the length of the wall (n = 8) for specimen RW2, and 19 uniaxial elements (n = 19) for specimen TW2. A refined configuration with 8 uniaxial elements was assigned for the flange specimen TW2, since the neutral axis was expected to be within the flange during loading subjecting the flange to compression. The tributary area on the cross-section assigned to each uniaxial element is also indicated on Fig. 4. As discussed in Orakcal [2], increasing the number of uniaxial elements or the number of MVLEs along wall height does not change significantly the prediction of the global response (i.e., lateral load versus wall story displacements); however, use of more MVLEs along wall height is valuable in terms of obtaining more detailed information on responses at a given location. Thus, the analytical model is refined for subsequent comparisons and discussions for local responses by modifying the number of MVLEs along wall height, depending on the location where a local response comparison between the analytical and experimental results is desired (e.g., LVDT locations, steel strain gauge locations, concrete strain gauge locations, wire potentiometer locations). For the refined analytical models, 16 MVLEM elements were used for the modeled walls (m = 16); with 8 elements along the first story height, 4 elements along the second story, and 2 elements along the third and fourth stories. A value of 0.4 was selected for the parameter c defining the center of relative rotation for each wall element, based on prior studies (Vulcano [1]). As discussed in Orakcal [2], using a large number of MVLEs along wall height, as has been done in this study, will diminish the influence of the parameter c on the predicted response.

Calibration for Material Properties

Steel Stress-Strain Relations

The reinforcing steel stress-strain relationship described by the Menegotto [5] model was calibrated to reasonably represent the experimentally observed properties of the longitudinal reinforcement used in the experimental study. These parameters also were used to calibrate the stress-strain relationship for the reinforcing bars in compression. The yield strength and strain-hardening parameters for the bare bars in tension were modified according to the empirical relations proposed by Belarbi [8] to include the effect of tension stiffening on steel bars embedded in concrete. Figure 6 shows the calibrated analytical steel stress-strain relations in tension and compression, as well as stress-strain test results for the reinforcement used in the construction of the wall specimens. The parameters accounting for the cyclic properties of the stress-strain relationship (R_0, a_1, a_2 in Fig. 2) were calibrated for the values suggested by Elmorsi [14] (R_0 = 20, a_1 = 18.5, a_2 = 0.0015) based on the experimental results carried out by Seckin [15]. As discussed by Dodd [16], the hysteretic properties of steel associated with the Bauschinger effect are sensitive to the carbon content of the steel, and thus, variations in the behavior are possible. The sensitivity of the model response with regard to these parameters is discussed in Orakcal [2].

Concrete Stress-Strain Relations

The monotonic envelope curves of the implemented concrete hysteretic stress-strain relation for compression and tension allow control on the shape of both the ascending and descending (i.e., pre-peak and post-peak) branches of the stress-strain behavior. The curves can be calibrated for selected values of peak stress, strain at peak stress, elastic modulus, and also via the parameter *r* defining the shape of the envelope curve, allowing for model refinement. The envelope curve used in the analytical model for unconfined concrete in compression was calibrated using results of the monotonic stress-strain tests conducted at time of testing on standard 152.4 mm x 304.8 mm cylinder specimens of the concrete used in the construction of the walls (Fig. 7(a)).

The concrete tensile strength was determined from the relationship $f_t = 0.31\sqrt{f_c'}$ (MPa), and a value of 0.00008 was selected for the strain (ε_t) at peak monotonic tensile stress; as suggested by Belarbi [8] based on a series of tests on RC panels with concrete cylinder compressive strengths (f_c') consistent with the compressive strength of concrete used for the construction of the present wall specimens. The *r*-parameter was calibrated in defining the shape of the monotonic tension envelope so that it reasonably agreed with the average post-crack stress-strain relation proposed by Belarbi [8] based on the effects of tension stiffening on concrete (Fig. 7(b)).

The compression envelope used in the analytical model for confined concrete was calibrated using the empirical relations proposed by Mander [17] for the peak compressive stress and the strain at peak compressive stress. The confined concrete stress-strain behavior was manipulated based on the area, configuration, spacing and yield stress of the transverse reinforcement (Fig. 6) in the confined regions within the first story height (0-0.91 m) of the test specimens. Accordingly, in the analytical model, the peak compressive stress (compressive strength of

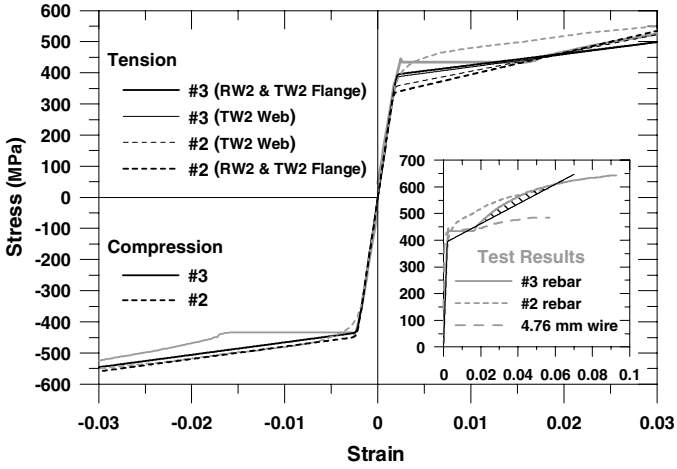

Figure 6 Steel Constitutive Model Calibration

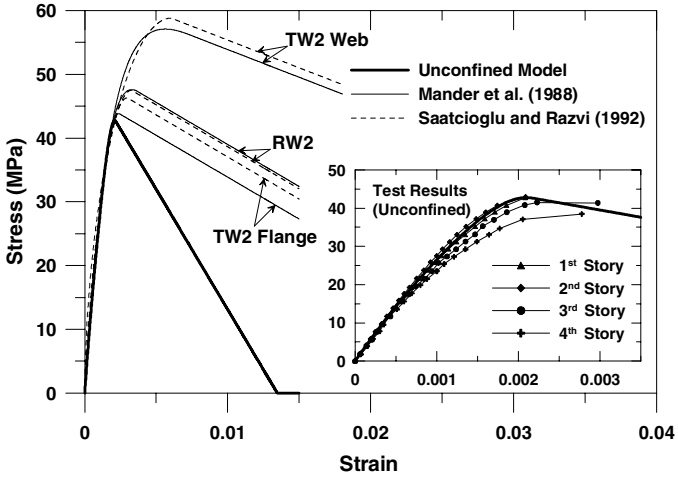

(a) Calibration for Compression

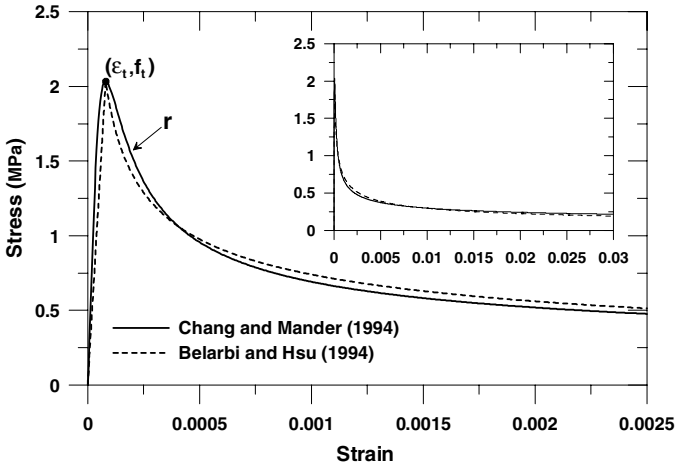

(b) Calibration for Tension

Figure 7 Concrete Constitutive Model

confined concrete) and the strain at peak compressive stress were modified within the confined concrete areas located at the edges of each wall. Figure 7(a) compares the monotonic stress-strain relations used in the wall models for confined and unconfined concrete with the relations proposed by Saatcioglu [18]. The strain ε_{cr}, where the monotonic stress-strain relation enters a linear stress degrading range after reaching the peak value, was calibrated such that the post-peak slope of the present stress-strain model agrees with the post peak slope of the Saatcioglu [18] model for both confined and unconfined concrete (Fig. 7(a)).

The hysteretic stress-strain rules defined by Chang [7] were used to simulate the cyclic behavior of both confined and unconfined concrete implemented in the wall model. The cyclic properties of the stress-strain relation by Chang and Mander are controlled by key hysteretic parameters including secant stiffness (E_{sec}) and plastic stiffness (E_{pl}) upon unloading from, and stress and strain offsets (Δf and $\Delta\varepsilon$) upon return to, the compression envelope (Fig. 3). An extensive column database was used by Chang [7] to develop empirical relationships for these parameters. The same empirical relationships were used in the present model as they were found to produce consistent results when used with the values specified for the remaining model and material parameters. Further details on the implemented concrete stress-strain relation can be found in Chang [7] and Orakcal [2].

Shear Force-Deformation Relation

The study presented herein focuses on modeling of the flexural responses, thus a linear elastic force-deformation behavior was adopted for the horizontal "shear" spring. The experimental results were separated into flexural and shear response components using the methodologies described in Massone [11]. In order to compare model results directly with the measured flexural responses, the stiffness of the shear spring (k_H) was assigned a very large (~infinite) value.

ANALYTICAL RESULTS AND COMPARISON WITH TEST RESULTS

The analytical model was implemented in Matlab [19] to allow comparison between experimental and analytical results. A displacement-controlled nonlinear analysis strategy was selected in order to correlate the model results with results of the drift-controlled cyclic tests subjected to prescribed lateral displacement histories at the top of the walls (Fig. 8). Prior to analysis, the lateral top displacement history applied during testing and the measured lateral story displacement histories for each specimen were corrected to remove displacement contributions resulting from shear and pedestal movement to allow for a direct comparison of the measured and predicted flexural responses. Measurements obtained in horizontal and vertical linear potentiometers mounted on the pedestals (Fig. 5) were used to remove displacements caused by pedestal rotation (caused by uplift) and pedestal sliding in the direction of the applied load.

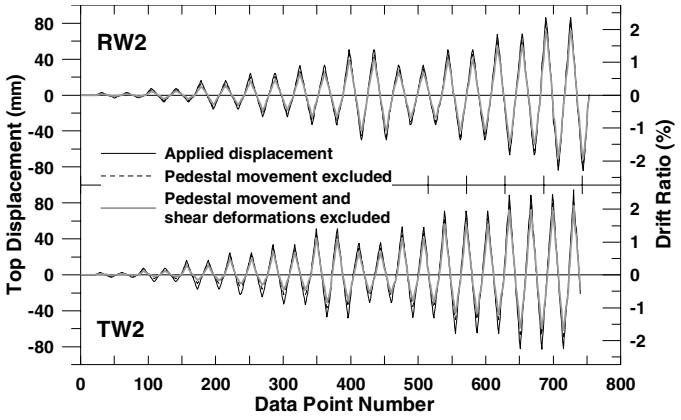

Figure 8 Top Lateral Displacement Histories

Wall shear deformations were calculated using data from wire potentiometers mounted on the bottom two stories of each specimen (Fig. 5) using the procedure recommended by Massone and Wallace [11]. The largest shear deformations were concentrated within the first story height of the wall, where shear yielding

was observed together with flexural yielding. The measured lateral load – shear deformation response in the second story was observed to follow an approximately linear elastic relationship; thus, the shear deformations in the third and fourth stories of the wall specimens were estimated for the entire loading history using the linear elastic shear stiffness values derived for the second story level. Figure 8 compares the lateral top displacement history applied to specimens RW2 and TW2 during testing, with lateral top displacement histories obtained after subtracting the contributions due to pedestal movement and shear deformations.

The analytical models for specimens RW2 and TW2 were subjected to the modified top displacement histories determined using the procedures outlined in the prior paragraph. The measured axial load histories applied on the wall specimens during testing, as measured by load cells during testing, were applied to the analytical models (on average, approximately 7% of the axial load capacity for RW2 and 7.5% for TW2, with variation of approximately $\pm$ 10%). Comparisons between model predictions of the flexural responses and test results are summarized for RW2 and TW2 in the following paragraphs. A discussion on the sensitivity of the analytical model results to the model and material parameters is presented in Orakcal [2].

Rectangular Wall, RW2

Figure 9 compares the measured and predicted lateral load – top flexural displacement responses for the rectangular wall specimen RW2. The analytical model captures reasonably well the measured response. Cyclic properties of the response, including stiffness degradation, hysteretic shape, plastic (residual) displacements, and pinching behavior are accurately represented in the analytical results; therefore, the cyclic properties of the implemented analytical stress-strain relations for steel and concrete produce good correlation for global response. The lateral capacity of the wall is predicted very closely for most of the lateral drift levels.

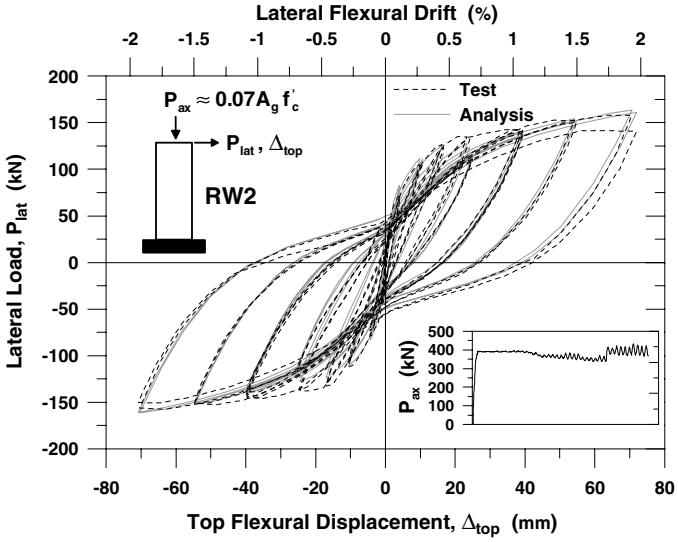

Figure 9 RW2 – Load-Displacement Response

The underestimation of the wall capacity at intermediate drift levels (e.g., 0.5 to 1.5 percent drift) can be attributed to the inability of the analytical stress-strain yield asymptote for steel in tension to model the curved strain-hardening region observed in the stress-strain tests for the #3 longitudinal reinforcing bars (see Fig. 7), as well as the uncertainty in the calibration of the cyclic parameters governing the implemented steel stress-strain relation (R_0, a_1 and a_2) and the parameters associated with concrete tensile strength (f_t and ε_t). Recalibration of the material parameters (e.g., $R_0 = 20$, $a_1 = 18.5$, $a_2 = 0.15$; and/or $f_t = 0.5\sqrt{f_c'}$ (MPa) and ε_t increased in proportion with f_t, with shape parameter r unchanged), would increase the predicted wall capacity for these intermediate drift levels and result in improved correlation. However, such recalibration would impair the correlation for the wall capacity at other drift levels, as well as the cyclic properties of the wall response including plastic (residual) displacements and pinching. The reader should refer to the paper by Orakcal et al. [2] for information on the sensitivity of model results to these material parameters.

Figure 10 shows a comparison of the lateral flexural displacements of the wall, at peak top displacement (top displacement reversal) data points for each drift level, measured by the horizontal wire potentiometers at the first, second and third story levels, (Fig. 5); with the results of the analysis. The analytical model provides a good prediction of the wall lateral displacement profile, and the distribution of deformations along wall height. The reader should note that the drift levels noted in the legend of Fig. 10, and in all subsequent figures, correspond to "nominal" drift levels applied to the wall during testing, versus actual drift levels (i.e., measured top displacement modified to remove contributions from pedestal and shear deformations).

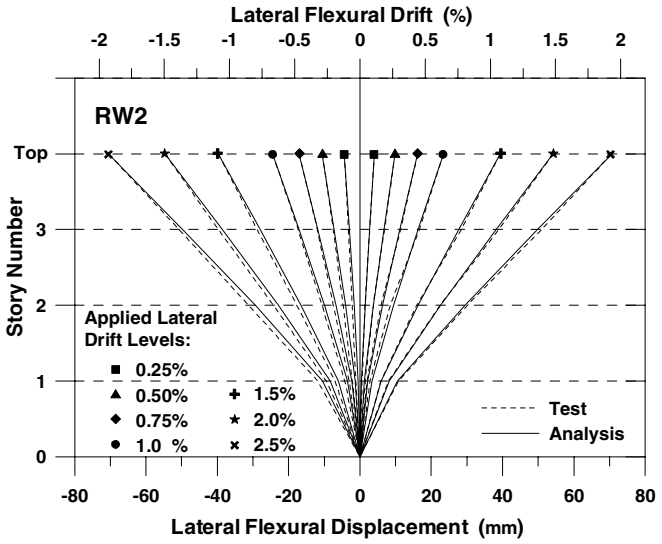

Figure 10 RW2 – Lateral Displacement Profiles

Figure 11 plots the measured and predicted lateral flexural displacement histories at the first story height (0.91 m) and the rotations accumulated over the bottom 0.76 m of the wall (rotations were measured via the two vertical wire potentiometers mounted to wall ends (Fig. 5)). Again, very good agreement between the experimental and analytical results is observed, indicating that the model successfully predicts the nonlinear flexural deformations experienced within the plastic hinge region of the wall.

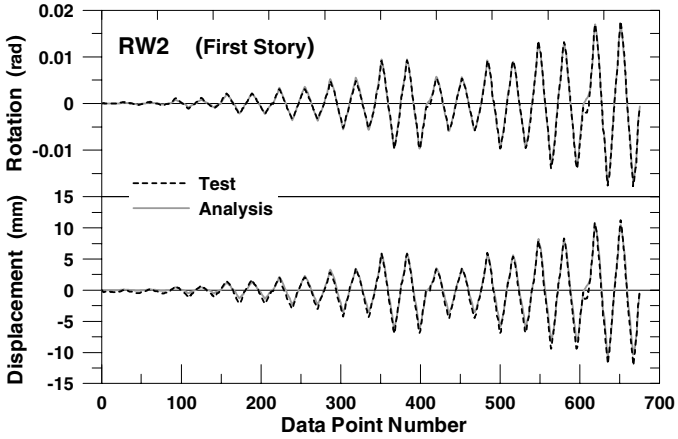

Figure 11 RW2 – First Story Deformations

Measured and predicted responses at specific locations are compared in Fig. 12, which plots the average concrete strains measured by the seven LVDTs over a 229 mm gauge length at the base of the wall (Fig. 5), at applied peak positive top displacement (top displacement reversal) data points, for selected drift levels applied during testing. Similar trends were observed in the results for other drift levels and also for peak negative top displacement data points. Results shown in Fig. 12 illustrate that the analytical model predicts reasonably well the tensile strain profile, but significantly underestimates the compressive strains. A similar correlation is observed for the strains in longitudinal steel bars (measured by steel strain gauges) at wall base level (Fig. 13), although the compressive strains in longitudinal reinforcement at the top of the first story level are

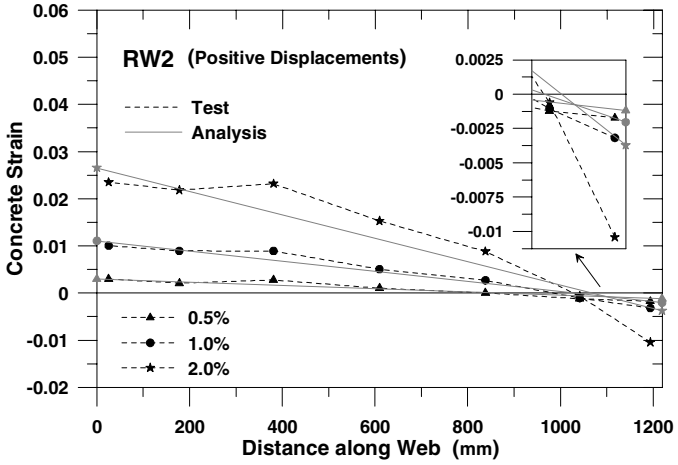

Figure 12 RW2 – Concrete Strain Distributions

predicted reasonably well. The larger measured compressive strains in concrete and longitudinal reinforcement located at the base of the wall may be due to stress concentrations induced at the wall-pedestal interface due to the abrupt change in geometry. As well, the larger compressive strains may be partially due to the nonlinear shear response that the wall specimen experienced within the first story height. Preliminary analysis results using a modified MVLE model with an implemented methodology for coupling shear and flexural displacements, based on biaxial constitutive relationships for concrete with compressive strain-softening, yields compressive strains larger than those predicted with the flexural model used here. Nevertheless, the underestimation of the compressive stresses does not apparently have a significant influence on the prediction of the global flexural response (Figs. 9-11) for the modeled wall and loading history used in this study.

Figure 14 compares measured responses for a specific gauge, an embedded concrete strain gauge with gauge length of 83 mm (Fig. 6), with results obtained with the model. The concrete strain gauge data were available up to data point number 330 (0.75% drift level), at which time the gauge failed. The analytical prediction again underestimates the measured compressive strains and overestimates the measured tensile strains (which are believed to be unreliable, as discussed below). Given the differences in the measured and predicted results, additional comparisons were made using strain histories measured by the LVDTs located on either side of the embedded concrete strain gauge. Results obtained with the two LVDTs straddling the embedded concrete strain gauge were used to estimate the strain at the location of the embedded concrete gauge using linear interpolation. Results are presented up to data point number 515, at which time the readings in the LVDT closest to the wall edge become unreliable. It is observed that the analytical tensile strain predictions are in very good agreement with the LVDT measurements in tension, as mentioned in the discussion of Fig. 12. The readings for the embedded concrete strain gauge are reasonably close to those obtained with the LVDTs for compressive strains, but the embedded gauge fails to measure correctly the tensile strains (it appears that bond between the embedded concrete strain gauge and the surrounding concrete is insufficient to measure accurately the large tensile strains that develop at wall boundaries). Similar data trends were observed for the concrete strain gauge located at the opposite wall boundary of specimen RW2. Overall, the results indicate that the analytical model underestimates the compressive strains, but predicts reasonably well the magnitude and variation of the

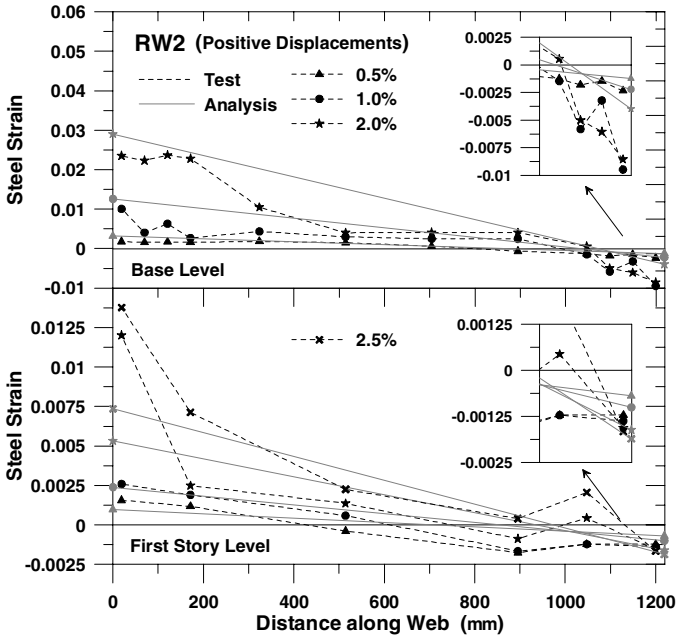

Figure 13 RW2 – Steel Strain Distributions

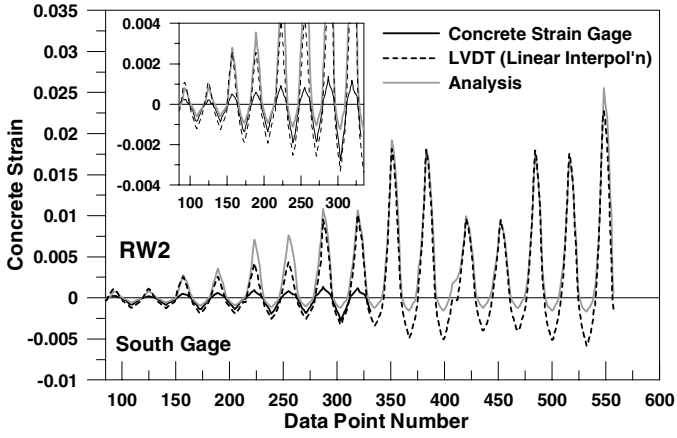

Figure 14 RW2 – Concrete Strain Histories

wall tensile strain histories, and that tensile strain measurements for the embedded concrete gauge are not reliable.

T-Shaped Wall, TW2

Figures 15 - 17 compare the analytical model predictions with selected experimental results for the T-shaped wall specimen TW2. The correlation of the analytical and experimental results for the lateral load – top flexural displacement response (Fig. 15), as well as first story displacement and rotations (Fig. 16) for TW2 resemble those for RW2, when the T-shaped specimen is subjected to displacements in the positive direction (when the wall flange is in compression). Therefore, the model provides a reasonably good prediction of the response for a T-shaped wall with the flange in compression, and the same conclusions noted for RW2 apply to TW2. This result implies that the plane section assumption, which assumes the entire flange is effective in compression for all drift levels, is appropriate.

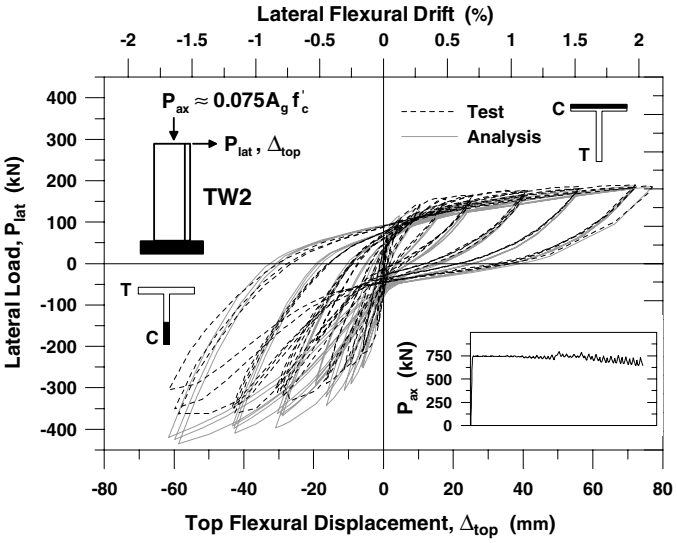

Figure 15 TW2 – Load-Displacement Response

However, for negative displacements (when the wall flange is in tension), the analytical model overestimates the lateral load capacity of the wall (Fig. 15), underestimates the lateral displacements at the first story level, and overestimates the rotations over the bottom 0.76 m of the wall. The reason for these discrepancies between the analytical and experimental results is the nonlinear tensile strain distribution experienced along the flange of the wall specimen during testing. The concrete strains (LVDT readings along the bottom 229 mm of the wall) and steel strains (steel strain gauge readings mounted on longitudinal reinforcement at wall base level), measured along the wall flange at peak top displacement data points, are plotted and compared with analytical results in Fig. 17 for selected drift levels. The measured tensile strains, both in steel and concrete, follow a nonlinear distribution along the width of the flange, which cannot be captured with the analytical model, which is based on a plane section assumption that produces a uniform tensile strain distribution along the flange. Because of this assumption, flange tensile strains are overestimated, leading to overestimation of the lateral load capacity of the wall when the flange is in tension. The experimentally observed nonlinear tensile strain distribution along the flange is also the reason for overestimation of the first story rotations and the underestimation of the first story displacements (Fig. 16) by the analytical model. The first story displacements predicted by the model are lower (despite overestimation of the inelastic rotations due to large tensile strains), because the length of the plastic hinge region (the height over which steel yielding is observed) is larger in the analytical model than that experienced by the wall specimen during testing. In contrast, the measured compressive strains along the

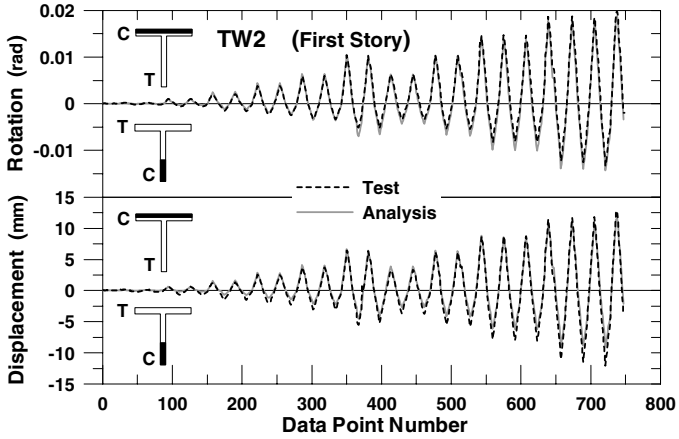

Figure 16 TW2 – First Story Deformations

flange (Fig. 17) are approximately uniform for all applied drift levels, resulting in fairly good analytical prediction of the global response for positive displacements.

SUMMARY AND CONCLUSIONS

The intent of this paper was to provide information on calibration of the Multiple-Vertical-Line-Element Model (MVLEM) and present comprehensive correlation studies between the analytically predicted and experimentally observed behavior of slender RC walls with rectangular and T-shaped cross sections at various response levels. State-of-the-art, robust constitutive relationships implemented into the MVLEM for concrete and reinforcing steel were calibrated based on the mechanical properties of the materials used in the construction of the walls modeled, and via parameters previously verified by other researchers (e.g., for confinement, tension stiffening, cyclic stress-strain behavior of steel and concrete). Wall test results were processed to exclude the contributions of pedestal movement and shear deformation components to allow for a direct comparison of the experimental results with the flexural response prediction of the analytical model. The analytical model was subjected to the same conditions experienced during testing (e.g., loading protocol, minor fluctuations in applied axial load). A refined configuration was used for the model in order to predict the responses at specific locations where instrumentation was provided for the tests. The correlation of the experimental and analytical results was investigated in detail, at various response levels and locations (e.g., story displacements, rotations over the first story level, average strains in steel and concrete).

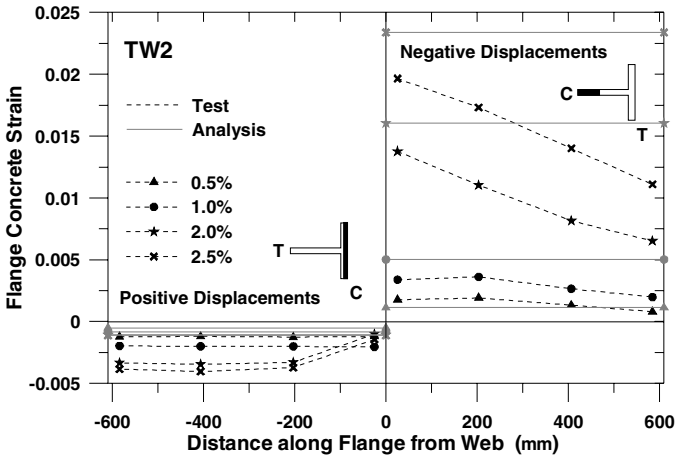

(a) Concrete Strains

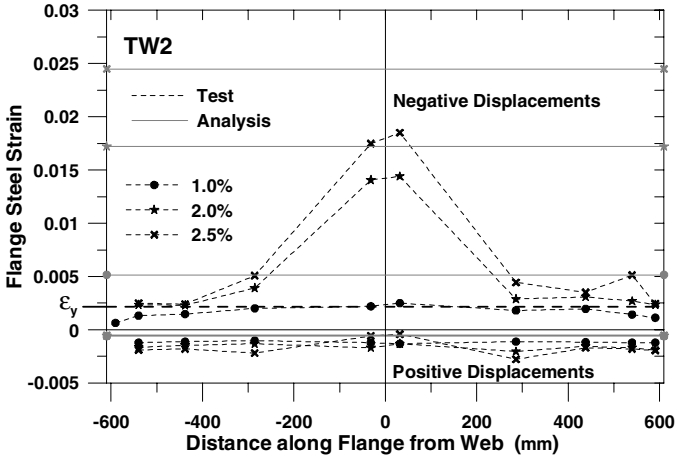

(b) Steel Strains

Figure 17 TW2 – Strain Distributions in Flange

It was observed that the MVLE model, as implemented here, provides a good prediction of the experimentally observed responses (wall lateral load capacity at varying drift levels, wall displacement profile, average rotations and displacements over the region of inelastic deformations) of the wall with rectangular cross section. The wall stiffness is well represented both prior to, and after wall yielding, and the yield point is captured effectively. The model provides a reasonably accurate prediction of wall tensile strains and the position of the neutral axis, whereas the compressive strains tend to be under-predicted, possibly due to stress concentrations at wall-pedestal interface or nonlinear shear deformations experienced within the nonlinear flexural deformation region of the wall. The authors recommend the selected constitutive relationships and the calibration methodology used in this study for a reliable prediction of the flexural response for slender RC walls with rectangular cross-sections.

The same level of accuracy is observed in the prediction of the global response for T-shaped walls when the flange is in compression, where the wall effectively behaves like a wall with a rectangular cross section. When the flange is in tension, discrepancies between the results obtained with the analytical model and the experimental results are observed for the wall lateral load capacity and the displacements and rotations along the wall. Wall lateral load capacity and inelastic rotations tend to be overestimated whereas inelastic lateral displacements are under-predicted, due to the observed nonlinear tensile strain distribution along the flange of the wall, which cannot be captured by the MVLE model as implemented in this study. For a reliable prediction of T-shaped wall response, modifications to the model to account for the variation of longitudinal strain along the wall flange. (e.g., via implementation of a nonlinear strain distribution relationship such as proposed by Pantazopoulou [20]). This is an area of current research by the authors.

This study focused on prediction of the flexural response of slender walls; however nonlinear shear deformations were observed in the slender the wall specimens tested, even though the peak applied lateral loads (wall shear forces) were only about one-half of the nominal shear capacity of the walls (see Massone [11]). Current work by the authors also focuses on developing a methodology to couple the flexural and shear displacement components.

Overall, the MVLE model, as used in this study, was shown to be an effective modeling approach for the flexural response prediction of slender RC walls, subject to the limitations mentioned above (which also apply for a two-dimensional fiber model). The model provides a flexible platform to assess the influence of various material and wall attributes on the nonlinear response of slender RC structural walls, as well as a practical platform for further implementing further improvements. Implementation of the model into a computational platform (e.g., OpenSees [21]) will provide design engineers improved analytical capabilities to model the behavior of structural walls and their interaction with other structural elements, which is essential for application of performance-based design.

ACKNOWLEDGEMENTS

The work presented in this paper was supported by funds from the National Science Foundation under Grants CMS-9632457 and CMS-9810012, as well as in part by the Earthquake Engineering Research Centers Program of the National Science Foundation under NSF Award Number EEC-9701568 through the Pacific Earthquake Engineering Research (PEER) Center. The test results used in this study were conducted by Dr. John H. Thomsen, now with SGH, Arlington, MA. The assistance of UCLA PhD students Mr. Leonardo Massone and Mr. Murat Melek are greatly appreciated. Any opinions, findings, and conclusions or recommendations expressed in this material are those of the authors and do not necessarily reflect those of the National Science Foundation.

REFERENCES

1. Vulcano; A., Bertero; V. V., and Colotti; V.; “Analytical Modeling of RC Structural Walls”; *Proceedings*; 9th World Conference on Earthquake Engineering; V. 6; Tokyo-Kyoto, Japan; 1988; pp. 41-46.
2. Orakcal; K., Wallace; J. W., and Conte; J. P.; “Nonlinear Modeling and Analysis of Reinforced Concrete Structural Walls”; *ACI Structural Journal*; 2004; accepted for publication.
3. Kabeyasawa; T., Shiohara; H., Otani; S., and Aoyama; H.; “Analysis of the Full-Scale Seven-Story Reinforced Concrete Test Structure”; *Journal of the Faculty of Engineering*; The University of Tokyo (B); V. 37; No. 2; 1983; pp. 431-478.

4. Vulcano; A., and Bertero; V. V.; "Analytical Models for Predicting the Lateral Response of RC Shear Walls: Evaluation of Their Reliability"; *EERC Report* No. UCB/EERC-87/19; Earthquake Engineering Research Center; University of California, Berkeley; 1987.
5. Menegotto; M., and Pinto; E.; "Method of Analysis for Cyclically Loaded Reinforced Concrete Plane Frames Including Changes in Geometry and Non-Elastic Behavior of Elements Under Combined Normal Force and Bending"; *Proceedings*, IABSE Symposium on Resistance and Ultimate Deformability of Structures Acted on by Well-Defined Repeated Loads; Lisbon; 1973.
6. Filippou; F. C., Popov; E. G., and Bertero; V. V.; "Effects of Bond Deterioration on Hysteretic Behavior of Reinforced Concrete Joints"; *EERC Report* No. UCB/EERC-83/19; Earthquake Engineering Research Center; University of California, Berkeley; 1983.
7. Chang; G. A., and Mander; J. B.; "Seismic Energy Based Fatigue Damage Analysis of Bridge Columns: Part I – Evaluation of Seismic Capacity"; *NCEER Technical Report* No. NCEER-94-0006; State University of New York, Buffalo; 1994.
8. Belarbi; H., and Hsu; T. C. C.; "Constitutive Laws of Concrete in Tension and Reinforcing Bars Stiffened by Concrete"; *ACI Structural Journal*; V. 91; No. 4; 1994; pp. 465-474.
9. Thomsen; J. H., and Wallace; J. W.; "Displacement-Based Design of Reinforced Concrete Structural Walls: An Experimental Investigation of Walls with Rectangular and T-Shaped Cross-Sections"; *Report* No. CU/CEE-95/06; Department of Civil Engineering, Clarkson University; Postdam, NY; 1995.
10. Thomsen IV; J. H., and Wallace; J. W.; "Experimental Verification of Displacement-Based Design Procedures for Slender Reinforced Concrete Structural Walls"; *Journal of Structural Engineering*; ASCE; 2003; accepted for publication.
11. Massone; L. M., and Wallace; J. W.; "Load-Deformation Responses of Slender Reinforced Concrete Walls"; *ACI Structural Journal*; 2003; accepted for publication.
12. Wallace; J. W.; "A New Methodology for Seismic Design of Reinforced Concrete Shear Walls"; *Journal of Structural Engineering*; ASCE; V. 120; No 3; 1994; pp. 863-884.
13. Wallace; J. W.; "Seismic Design of Reinforced Concrete Shear Walls; Part I: New Code Format"; *Journal of Structural Engineering*; ASCE; V. 121; No. 1; 1995; pp.75-87.
14. Elmorsi; M., Kianush; M. R., and Tso; W. K.; "Nonlinear Analysis of Cyclically Loaded Reinforced Concrete Structures"; *ACI Structural Journal*; V. 95; No. 6; 1998; pp. 725-739.
15. Seckin; M.; "Hysteretic Behavior of Cast-in-Place Exterior-Beam-Column-Slab Sub-assemblies"; *Dissertation*; University of Toronto, Canada; 1981.
16. Dodd; L. L., and Restrepo-Posada; J. I.; "Model for Predicting Cyclic Behavior of Reinforcing Steel"; *Journal of Structural Engineering*; ASCE; V. 121; No. 3; 1995; pp. 433-445.
17. Mander; J. B., Priestley; M. J. N., and Park; R.; "Theoretical Stress-Strain Model for Confined Concrete"; *Journal of Structural Engineering*; ASCE; V. 114; No. 8; 1988; pp. 1804-1826.
18. Saatcioglu; M., and Razvi; S. R.; "Strength and Ductility of Confined Concrete"; *Journal of Structural Engineering*; ASCE; V. 118; No. 6; 1992; pp. 1590-1607.
19. "Matlab"; *The Math-Works, Inc.*; Natick, Massachusetts; 2001.
20. Pantazopoulou; S. J., and Moehle; J. P.; "Simple Analytical Models for T-Beams in Flexure"; *Journal of Structural Engineering*; ASCE; V. 114; No. 7; 1988; pp. 1507-1523.
21. "OpenSees – Open System for Earthquake Engineering Simulation"; *Pacific Earthquake Engineering Research Center*; University of California, Berkeley. (http://opensees.berkeley.edu/OpenSees/developer.html)